International Journal of Fracture, Vol. 9, No. 2, June 1973
Noordhoff International Publishing–Leiden
Printed in The Netherlands

A model for unstable shear crack propagation in pipes containing gas pressure

G. T. HAHN, M. SARRATE*, M. F. KANNINEN AND A. R. ROSENFIELD

Battelle Columbus Laboratories, 505 King Avenue, Columbus, Ohio 43201

(Received November 26, 1971; in revised form January 11, 1972)

ABSTRACT

A tentative analysis of an unstable shear crack propagating axially in the wall of a long pipe under gas pressure is developed. Six processes known to be associated with crack propagation are treated numerically: (1) axial decompression of the gas, (2) bulging of the pipe wall, (3) radial decompression of the gas, (4) local stress and strain intensification at the crack tip, (5) plastic deformation, and (6) ductile cracking. The treatment is quasi-static; dynamic effects in the pipe wall are ignored. Because the numerical descriptions included in the model are approximate and incomplete, several variants of the basic model are examined. The response of the model is evaluated for different line pressures, geometries, and material properties and compared with full-scale test data for 100% shear cracks. A wide range of speeds can be calculated for the limits within which the system parameters are specified including the speeds observed in practice. The bulging and decompression characteristics of the model cause the crack speed to be relatively insensitive to line pressure. Yet the calculated crack speeds are influenced by yield strength and toughness of the material. The model does not provide for nonaxial crack paths, nor does it adequately describe crack-arrest possibilities. The paper represents the first step in the analysis of a complex problem.

1. Introduction

The speed and path of an unstable crack in the wall of a pipe under pressure affects the length of fracture** [1]. To learn more about this problem. McClure, Duffy and Eiber [1–5] have made full-scale tests of the pipe sizes, steels, and pressures employed in natural gas transmission lines under sponsorship of the Pipeline Research Committee of the American Gas Association (Project NG-18). Their work shows that 100% shear cracks propagate at speeds ranging from 400–800 fps for X-52 and X-60 grades to 800–1200 fps for higher strength quenched and tempered grades. Initially, such failures follow a straight, axial path, but tend to veer into a helical trajectory which greatly reduces the axial and actual path component of velocity and the length of pipe damaged. Surprisingly enough, the line pressure (or hoop stress) seems to have no clearly discernible effect on speed or trajectory; neither were systematic effects assigned to backfill or pipe geometry (the ratio of radius to wall thickness), though the latter was examined only in a limited way covering only the diameters and wall thicknesses in general use for gas transmission pipelines.

While the full-scale tests have exposed the main features of crack propagation in pipes, they do not, by themselves, explain the speeds and trajectories observed. Only limited progress has so far been made in this direction. McClure and co-workers [3] have shown analytically that a certain class of elastic waves, which can propagate in cylinders, have speeds and trajectories similar to cleavage cracks. The principles that govern the selection of particular waves was not worked out in detail. It also seems unlikely that elastic waves will interact strongly with the slower moving shear fractures, and no other explanation for the mechanisms controlling shear cracks has been proposed. Yet, the shear mode is important technologically, since shear fractures have been observed to propagate unstably.

* Argentine Atomic Energy Commission.

** When the axial propagation speed of a crack is comparable to or exceeds the speed of decompression, then the crack front does not experience a pressure loss. Since the hoop and bending stresses that drive the crack are largely maintained in this case, the "fast" crack tends to produce a long failure. In contrast, the "slow" crack—one that lags far behind the decompression event—experiences the loss of pressure in the line. This can reduce the driving force for cracking sufficiently to produce crack arrest.

This paper takes the first step towards assembling a treatment of shear crack propagation from numerical descriptions of the six underlying processes:

(1) Axial decompression
(2) Bulging
(3) Radial decompression
(4) Local stress and strain intensification
(5) Plastic deformation
(6) Ductile cracking

The treatment is quasi-static; dynamic effects on the pipe wall may well be important but are difficult to handle and have not been included. The descriptions of bulging and stress intensifications are derived for an axial crack and do not consider nonaxial paths. It should therefore be clear that a highly idealized fracture event is being treated with an imperfect model. Thus, while some of the features of the model are in accord with experience, others are apparently contradicted by data from full-scale tests.

2. Numerical Descriptions

The treatment of shear fracture described recognizes the 6 processes which are shown schematically in Figure 1:

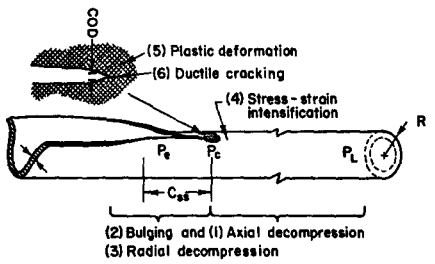

Figure 1. Schematic representation of a fracturing pipe identifying the processes underlying crack propagation.

(1) *Axial Decompression*

This term refers to the difference between P_L, the line pressure before failure, and P_c, the pressure existing near the tip of the propagating crack. The pressure difference arises from the loss of gas through the rupture and depends on the speed of decompression waves in the gas relative to the speed of the crack.

(2) *Bulging*

The term bulging is used to refer to the radial, out-of-round distortion of the unsupported pipe wall on either side of the crack. As a result of the bulging, the pipe wall develops a radial component of velocity that depends on the extent of the bulging and the forward speed of the crack. This bulging also places a limit on c_{ss}, the steady-state crack length in that portion of the pipe that can still be regarded as a pressure-containing vessel.

(3) *Radial Decompression*

This process leads to the difference between P_c and the effective pressure P_e acting on the bulging pipe wall. This difference is a consequence of the radial velocity of the bulging wall relative to the velocity of the gas molecules. In the actual case, the difference between P_c and P_e may be insignificant within the steady-state crack length distance; some full-scale data seem to indicate this. However, for the purposes of this analysis, P_c and P_e are viewed as separate parameters.

(4) *Local Stress and Strain Intensification*

The hoop and bending stresses acting on the cracked wall produce a plastic zone surrounded by an intense stress field at the crack tip. The COD (crack opening displacement) is a measure

of the plastic strains within the zone and this depends on the flow strength of the pipe and the stress field intensity.

(5) *Plastic Deformation*
The plastic deformation of steels is a rate-sensitive process. The flow strength of material within the plastic zone, and consequently the COD, therefore depend on the velocity of the crack.

(6) *Ductile Cracking*
The extension of a ductile crack by either the shear or the fibrous mode is associated with a critical COD, i.e., a critical crack opening displacement and K_c, a critical stress field intensity, which correspond with a critical level of plastic strain in the locale of the crack.
These 6 processes are discussed and formulated in the following sections.

3. Axial Decompression

McClure, Eiber and Duffy [1, 3] have examined axial decompression in pipes. Their measurements provide the basis for the following simple expression* for P_c, the pressure just ahead of an opening in the pipe wall traveling axially at a speed U:

$$P_c = \begin{cases} P_L \left[1 - 0.72 \left(1 - \dfrac{U}{U_g}\right)\right], & U < U_g \quad (1A) \\ P_L, & U \geqq U_g \quad (1B) \end{cases}$$

where U_g is the speed of a decompression wave in the gas at the operating temperature. For the purposes of the calculations in this paper, it was assumed that $U_g = 1500$ fps, a value approximately 12 percent higher than for natural gas at ambient temperatures, but necessary to make the simpler linear assumption for axial decompression fit the actual measured data of Athens Test 20 [1]. Equation (1A) also satisfies the theoretical limit for a stationary opening, i.e., $P_c = 0.28\ P_L$. Finally, since P_c is not likely to be established instantaneously, the following linear interpolation was used to characterize the period between the onset of cracking ($P_c = P_L$) and the achievement of the steady state:

$$P_c = P_L \left[1 - 0.72 \left(\frac{C - C^*}{C_{ss} - C^*}\right)\left(1 - \frac{U}{1500}\right)\right] \quad (1C)$$

where C^* is the crack length at the onset of propagation and C_{ss} the steady-state crack length discussed in the next section. This linear interpolation, which serves to characterize the transient period, is an arbitrary simplifying assumption. It presupposes that the crack extension needed to achieve steady state and C_{ss}, the effective length of the crack at steady state, are one and the same. In actual fact, calculated C_{ss}-values are about 1 pipe diameter while full-scale experiments indicate that steady-state decompression is not achieved within 3–5 pipe diameters.

4. Bulging

In the absence of more refined treatments, it is assumed that the bulging of the pipe wall on either side of the crack is similar to the deflection of classical, cantilevered beams subjected to a uniformly distributed load P, corresponding to the pressure in the pipe. To simplify matters further, the extent of bulging is described with a single parameter, $B \equiv \delta/C$, which is referred to here as the bulge deflection. As shown in Figure 2, δ corresponds to the beam deflection, while the crack length, $2C$, corresponds to the beam span. The beam-analogs provide insight to the

* A nonlinear relation obtained from one-dimensional gas dynamics has been found to predict actual pressure measurements in full-scale experiments extremely accurately. However, in this tentative analysis, it is more convenient and sufficiently accurate to use the linear form given above.

functional relations likely to exist between B and the crack length C, the pipe geometry R and t, and the pressure P:

$$B = \beta_1 \left(\frac{PR}{Et}\right)^m \left(\frac{C}{t}\right)^n , \tag{2}$$

where E is the modulus and β_1 is a numerical constant. As an example, consider as the analog of a pipe, a beam (or plate) under a uniform pressure P, with three edges built in and one edge free. The solution is given by Timoshenko and Woinowsky–Krieger [7]. In this case, $m=1$, $n=2$, and $\beta_1=0.5$; consider also a pipe for which $R=15$ in., $t=0.312$ in., and $E=30\times10^6$ psi, and a propagating shear crack for which the steady-state crack length and pressure are $C_{ss}\sim15$ in., $P\sim300$ psi*. Inserting these values into Equation (2) gives $B=0.55$, and this can be compared with a photograph of a propagating shear failure in an X-100 steel pipe: $R=15$ in., $t=0.312$ in. published by Duffy *et al.* [4], which shows an inclination of the pipe wall near the crack tip consistent with $0.2\lesssim B\lesssim0.8$**. At present, it is not possible to establish the value of B much more precisely than this, and so it is treated as a parameter whose maximum value is disposable within the range $B=0.2$ to 0.8. The calculations employ β_1-values consistent with these limits and $m=1, 2$ and $n=1, 2$ to show the effect of different dependencies on the behavior of the crack. Values of $m>1$ correspond to situations where the bulging involves plastic as well as elastic deformation.

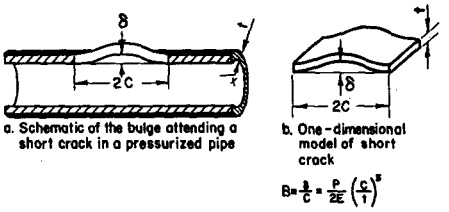

Figure 2. Schematic representation of the bulge of cracked pipe: (a) pipe, and (b) beam analogue.

The quantity B can also be regarded as a rough measure of the average inclination of the pipe wall on either side of the crack relative to the pipe axis (see Figure 2***). It thus defines U_R, the average radial velocity of the bulging pipe wall:

$$U_R \approx BU , \tag{3}$$

where U is the axial speed of the crack (since bulge travels with the crack). This simple picture also identifies the quantity R/B which can be interpreted as the distance from the crack tip to the point where the crack opening is comparable to the pipe diameter. Beyond this point, the structure is more like a U-shaped ribbon than a cracked pipe. The bulge deflection thus provides a basis for estimating C_{ss}, the steady-state crack length:

$$C_{ss} \approx \beta_2 \frac{R}{B} , \tag{4}$$

where β_2 is approximately constant and close to unity. The term C_{ss} is defined as above, or taken as a small multiple of the pipe radius independent of B, to simplify the calculations further.

5. Radial Decompression

The pressure P_e (or effective pressure) exerted by a gas on a containment wall that is moving depends on U_w, the velocity of the wall, relative to U_g, the velocity of the gas molecules:

* These estimates are derived from the calculations discussed in subsequent sections.

** Considerable uncertainly must be placed on this comparison because the circumferential weld failed before the arrival of the axial fracture. This, of course, would affect the way in which the pipe op·ned up.

*** This is a simplified, two-dimensional view of what is properly a three-dimensional problem.

$$P_e = P_s \left[\frac{U_g - U_w}{U_g}\right]^2, \tag{5}$$

where P_s is the pressure that would be exerted if the wall were stationary. Translated into the context of the bulging pipe, U_R is equated with U_W, and P_c with P_s:

$$P_e = P_c \left[\frac{U_g - BU}{U_g}\right]^2. \tag{6}$$

The quantity P_e is here regarded as the driving force for crack propagation even though this pressure is only applied to the bulge and not the entire pipe. This is not unreasonable since, as shown in the next section, the out-of-plane bending within the bulge dominates stress intensification at the crack tip. To simplify matters further, it is assumed that $U_g = 1100$ fps, a value that is intended to reflect the adiabatic expansion experienced by the gas in the bulging region.

6. Stress-Strain Intensification

The stress field at the tip of the propagating crack is here treated as a quasi-static problem and formulated by the procedure outlined in Reference 8, which has been adopted by several authors [9–11]. This assumes that a through-cracked pipe under pressure is equivalent to a cracked, semi-infinite flat plate loaded in simple tension to a nominal stress σ, that is a multiple M of the hoop stress

$$\sigma = M\sigma_H \tag{7}$$

$$M = \begin{cases} \left[1 + 1.61\,\dfrac{C^2}{Rt}\right]^{\frac{1}{2}}, & \dfrac{R}{t} \lesssim 50 \quad (8) \\[2ex] \left[1 + 1.61\,\dfrac{C^2}{R^2}\right]\left(50 \tanh \dfrac{R}{50t}\right)\Bigg]^{\frac{1}{2}}, & \dfrac{R}{t} \gtrsim 50 \quad (9) \end{cases}$$

and

$$\sigma_H = \frac{P_e R}{t}. \tag{10}$$

Note here that the contribution of bulging, $(M-1)/M$, is much greater for long cracks than the contribution of the hoop stress, $1/M$, and this justifies the use of P_e in Equation (10).

7. Plastic Deformation

Plastic deformation produced ahead of the propagating crack must occur at very high rates. This can be seen by noting the relation between the average strain rate $\dot{\varepsilon}$, and the crack speed U:

$$\dot{\varepsilon} = \left(\frac{\Delta\varepsilon}{\Delta x}\right) U, \tag{11}$$

where $\Delta\varepsilon/\Delta x$, the average plastic strain gradient ahead of the crack is likely to be in the range 2 in.$^{-1}$ to 25 in.$^{-1}$. This means that $\dot{\varepsilon} \approx 1.2 \times 10^4 - 1.5 \times 10^5 \,\text{sec}^{-1}$ for a crack propagating at 500 fps. The flow stress, $\bar{\sigma}$, of steel under these conditions is likely to be $2\times$ to $3\times$ the value measured in an ordinary tensile test [13–20], and this will influence the magnitude of the COD, as described in the next section.

Following the procedure in Reference 21, the rate dependence is approximated by a simple linear relation:

$$\bar{\sigma} = \bar{\sigma}_s + F\dot{\varepsilon}, \tag{12}$$

where $\bar{\sigma}_s$ is the static flow stress and is regarded as the average between the yield stress and ultimate tensile stress for the purposes of this paper, and $F \approx 2$ psi sec. Comparisons with recent measurements [13–19] show that Equation (12) does not offer a very satisfactory

description of actual test data. The interpretation is complicated by twinning, which is not very prevalent in fine-grained pipe steels but may have reduced the strength levels observed by Rhode [19] and by Oxley and Stevenson [17] at the highest strain rates. It should also be noted that $\Delta\varepsilon/\Delta x$ is not well known, and that this quantity may also vary with the rate of deformation. For the purposes of this report $\Delta\varepsilon/\Delta x$ is treated as disposable within the range 2 in.$^{-1}$ to 25 cm^{-1}.

8. Ductile Cracking

Crack extension by either the shear (plane stress) or fibrous mode (plane strain) is thought to occur when the highly strained region just ahead of the crack reaches a critical size. This condition is associated with a characteristic COD* (critical crack opening displacement) or K_c (critical stress field intensity), which are related:

$$\text{COD}^* \approx \frac{K_c^2}{\beta_3 E \bar{\sigma}_s} = \frac{\sigma^2 \pi C^* \varphi}{\beta_3 E \bar{\sigma}_s}, \tag{13}$$

where

$$\varphi = \left(\frac{\pi\sigma}{2\bar{\sigma}}\right)^{-2} \ln\left(\sec\frac{\pi\sigma}{2\bar{\sigma}}\right)^2 \tag{14}$$

and $\beta_3 = 1$ for plane stress and $\beta_3 = 2$ for plane strain. These expressions are valid for flat plates and can be applied to pipes by making use of the equivalences expressed by Equations (7)–(10).

These concepts are extended to propagating cracks, via the assumptions that changes in the strain distribution that accompany crack propagation can be neglected, at least to a first approximation. It follows from this that COD* is independent of the crack speed* [21, 22] and that the increase in crack length attending crack propagation is balanced by the increases in the flow stress prescribed by Equations (11) and (12) [21, 22]:

$$U = \frac{\bar{\sigma}_s}{\left(\frac{\Delta\varepsilon}{\Delta x}\right) F}\left[\frac{\sigma^2 \pi C \varphi}{\beta_3 E\, \text{COD}^*\, \bar{\sigma}_s} - 1\right] = \frac{\bar{\sigma}_s}{\left(\frac{\Delta\varepsilon}{\Delta x}\right) F}\left[\frac{\sigma^2 \pi C \varphi}{K_c^2} - 1\right]. \tag{15}$$

This assumption is not on very firm ground. For example, there are indications that shear crack propagation can be an intermittent process with instantaneous crack speeds much higher than the average [22]. Under these circumstances, inertia effects centered about the crack tip, which are ignored here, may be regulating the crack speed. There is also evidence for a 3-fold increase in COD* accompanying full-shear crack propagation in steel foils [21]. While no attempt is made to factor a COD* variation into the analysis, the possibility can be represented by a larger-than-actual $(\Delta\varepsilon/\Delta x)$-value which has the effect of an increasing COD*. The problem is that the strain gradient is not known precisely enough to make this a meaningful exercise.

9. Theoretical Models

The numerical descriptions given in the preceding paragraphs are summarized in Table 1A of the Appendix. This shows more clearly that the following inputs:

geometric factors: R, t, β_1, m, n, β_2 (or C_{ss}), and β_3

material properties: K_c (or COD*), E, $\bar{\sigma}_s$, F, and $\Delta\varepsilon/\Delta x$

operating condition: P_L

fully determine the remaining 5 unknowns: C^*, P_e, B, C_{ss}, and U (including U_{ss}). The quantities β_1, m, n, β_2 (or C_{ss}), and $\Delta\varepsilon/\Delta x$ are not well known and to some extent, disposable. For this reason, calculations were performed for different combinations of these parameters which are

* This means that K_c increases with crack speed because it depends on the flow stress (Equations (11), (12) and (13)): $K_c \approx \{\beta_3 E\, \text{COD}^* [\bar{\sigma} + (\Delta\varepsilon/\Delta x) F U]\}^{\frac{1}{2}}$.

TABLE 1

Description of crack-propagation models

Model No.	m	n	β_1	β_2	C_{ss}, *in.*	$\Delta\varepsilon/\Delta x$, *in.*$^{-1}$
1J	1	1	26.3	0.47	—	10
2J	1	2	0.66	0.47	—	10
3J	2	2	1120	0.40	—	10

given in Table 1. Each set is regarded as a slight variant of the general model of the fracturing pipe.

The properties of these models were obtained for different pipe geometries, material properties, and line pressures, with most of the calculations for a standard geometry: $R=15$ in., $t=0.375$ in., and a "standard" steel with properties similar to the X-60 line pipe grade:

TABLE 2

Properties of the "standard" steel

$E = 30{,}000{,}000$ psi
$\sigma_Y = 60{,}000$ psi
$\bar{\sigma}_s = 76{,}000$ psi
$F = 2$ psi sec
$K_c = 400$ ksi in.$^{\frac{1}{2}}$ (Reference 8)
$\beta_3 = 1$
COD* = 0.070 in.

10. Results

The general features of the models are illustrated in Figures 3–8. The critical crack length, C^*, is smaller and calculated crack speeds are greater in the pipe than in a comparable flat plate. This is a consequence of the radial forces which bulge the pipe wall and intensify the stress field at the crack tip. At high speeds, the forces communicated to the bulge are limited by the radial decompression phenomenon and this serves to moderate the crack speed.

It is important to note that a wide range of steady-state speeds can be calculated for the

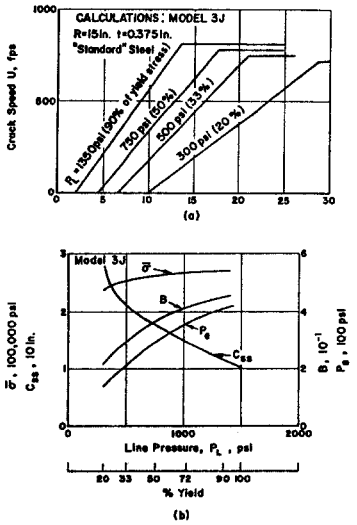

Figure 3. Calculated influence of line pressure: (a) during initial period of acceleration, and (b) at steady state.

limits within which n, m, β, $(\Delta\varepsilon/\Delta x)$, F, and C_{ss} can be specified, including the speeds observed in practice. In general, larger values of $\Delta\varepsilon/\Delta x$ and β_1 reduce U_{ss}, while larger values of C_{ss} raise U_{ss}; the values of M and N affect the initial rate of acceleration, the line-pressure dependence and other features which are discussed later. Figure 3 shows the kind of values attributed by the calculations to the parameters P_e, B, C_{ss}, and $\bar{\sigma}$ under steady-state conditions:

$$P_e \sim 175\text{–}400 \text{ psi} \qquad C_{ss} \sim 0.6R\text{–}1.5R$$
$$B \sim 0.2\text{–}0.6 \qquad \bar{\sigma} \sim 200\text{–}400 \text{ ksi}.$$

In view of the uncertainties, the functional relations predicted by the models are at this stage more meaningful than the absolute values of crack speed. The relation between P_L and U_{ss} is especially interesting. Here, untutored intuition would suggest a strong dependence on P_L,

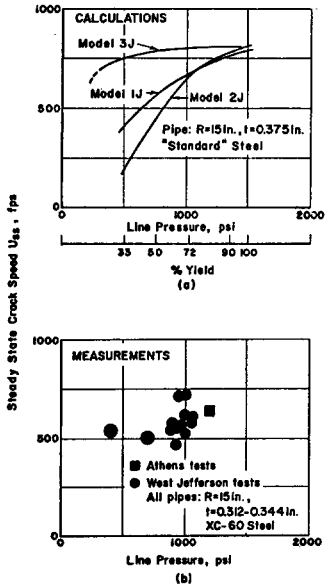

Figure 4. Influence of line pressure on the speed of 100% shear cracks: (a) calculated values, and (b) measured values obtained by Duffy and co-workers [23].

yet the significant body of test experience in Figure 4b amassed by Duffy and co-workers [1] shows that U_{ss} is relatively insensitive to P_L. Figure 4a illustrates that Model 3J displays the same (relative) insensitivity to P_L. This is because high values of P_L produce large bulge deflections which tend to reduce C_{ss} and moderate P_e through radial decompression; small P_L values, on the other hand, involve larger C_{ss}-values (see Figure 3b) which tend to compensate for the reduction in P_e. In other words, the mechanics of bulging and decompression attributed to the model provide built-in compensation for changes in line pressure.

Figure 3b illustrates for Model 3J, that the C_{ss}-value prescribed by the pipe opening criterion, Equation (4), increases rapidly for line pressures below 300 psi (20% of yield). In this case the criterion is probably invalid since a total pressure loss could be achieved even before the pipe has opened the required amount. For this reason, the rapid increase in C_{ss} is regarded as a sign that it is difficult to sustain steady-state propagation below the indicated pressure. Model (3J), which is least sensitive to pressure, simulates plastic bulging, and this seems to be in accord with photographs showing that the fractured pipes retain their bulged configuration after failure [1]. Figure 3a also illustrates the dependence of C_{ss} on P_L.

Figures 5 and 6 show the calculated influence of pipe geometry on steady-state speed. For Models (2J) and (3J), U_{ss} increases with increasing radius, mainly because of the dependence of C_{ss} on R (see Equation (4)). However, these models give contradictory results for the influence of wall thickness at constant radius (Figure 6a). Furthermore, full-scale test data indicate that U_{ss} is essentially independent of R in the range shown in Figure 5a. Thus, while Model 3J seemingly is consistent with full-scale data relative to the insensitivity of the pressure, it does not

give results consistent with full-scale data relative to pipe radius and wall thickness.

Figures 7a and 8 illustrate the separate effects of strength level and toughness on steady-state speed. In the first case it is assumed that increases in strength level are utilized in terms of higher P_L-values (hoop stresses are 72% of the yield stress), which, in turn, lead to faster cracks. Thus, higher strength levels must be matched by higher toughness values if U_{ss} is to remain unaffected. Increases in K_c at constant strength level reduce U_{ss} mainly through the increase in C^*. The

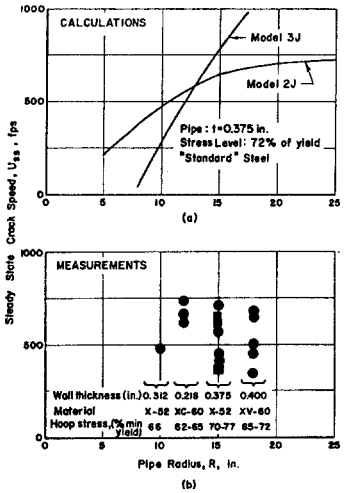

Figure 5. Influence of pipe diameter on the speed of 100% shear cracks: (a) calculated values, and (b) measured values obtained by Duffy and co-workers [23].

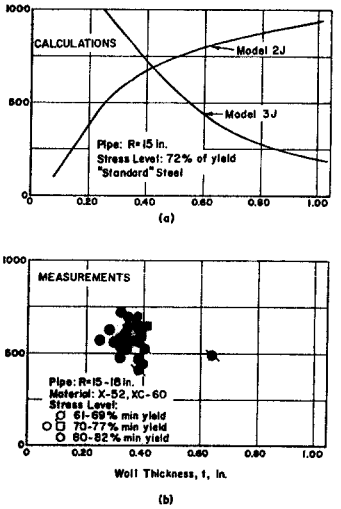

Figure 6. Influence of wall thickness on the speed of 100% shear cracks: (a) calculated values, and (b) measured values obtained by Duffy and co-workers [23].

models thus reproduce the main effect of the shear-to-cleavage transition which changes K_c from $\sim$400 ksi in.$^{\frac{1}{2}}$ for shear to $\sim$100 ksi in.$^{\frac{1}{2}}$ and less for cleavage. Figure 8 illustrates that such a toughness change produces a very large increase in crack speed, consistent with experience. The 5–8 fold increases calculated with Models 2J and 3J are to some extent exaggerated because speeds in excess of 1000–1500 fps probably invoke additional speed-moderating dynamic effects which have not been taken into account. It should also be noted that the larger increases in strength level are likely to be accompanied by reductions in K_c. The combined effect of strength level and toughness changes is calculated in Table 3.

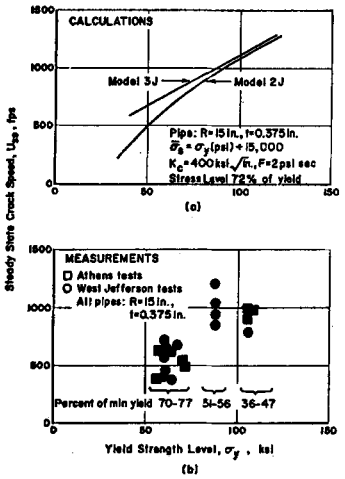

Figure 7. Influence of yield strength level on the speed of 100% shear cracks: (a) calculated values, and (b) measured values obtained by Duffy and co-workers [23].

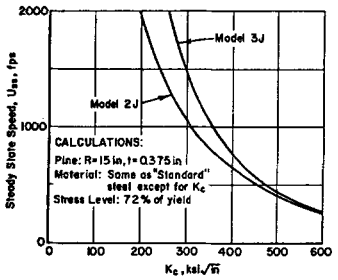

Figure 8. Calculated influence of fracture toughness on steady-state crack speed.

TABLE 3

*Calculated influence of strength level and attendent toughness on steady-state crack speed**

σ_Y, ksi	K_c, ksi in.$^{\frac{1}{2}}$	*Steady State Speed, fps*	
		Model 2J	*Model 3J*
40	475	200	400
60	400[a]	653	790
60	100[b]	>2000	>2000
100	400	1105	1120
150	250	>2000	>2000

* Calculated for $R=15$ in., $t=0.375$ in., $E=30{,}000$ ksi, and $F=2$ psi sec.
[a] Approximation of the toughness level associated with 100% shear fracture.
[b] Approximation of the toughness level associated with 100% cleavage fracture.

11. Discussion

The predictions of the models are compared in Figures 4b, 5b, 6b, and 7b with crack speed measurements on 100% shear cracks performed by Duffy and coworkers [22]. The comparisons illustrate that the models have many features in common with full-scale pipe failures.

1. *Line Pressure*

The line pressure (or hoop stress) dependence of U_{ss} is similar (Figure 4).

2. *Yield Strength Level*
The dependence of U_{ss} on yield strength (and hoop stress) level is similar (Figure 7)★.

3. *Toughness Level*
The change in crack speed accompanying the change in fracture toughness associated with the shear-to-cleavage transition is similar. (Figure 8 and Table 3).

At the same time, it should be clear that the descriptions used are all more or less approximate, and while some of the errors may cancel out, discrepancies remain. For one thing, it seems likely that the rate sensitivity of the flow strength is overestimated by the linear expression used. There is some evidence that the stress intensification produced by long cracks is also overestimated [24–26]. The effects of higher strength and higher stress thus tend to cancel. Several discrepancies are revealed by the comparisons with full-scale test data. The calculated influence of pipe radius does not seem to match the existing test experience and neither of the two calculated trends with thickness appear to be good representations of the data. The fact that Models 2J and 3J in Figure 6 give contradictory results is a sign that the exact forms of the expressions for B and C_{ss} are quite critical. In addition to these problems, there are two other shortcomings that stand in the way of calculating crack arrest: (1) the models only provide for the axial crack path and (2) the description of C_{ss} does not take into account the rate at which pressure is lost through the ruptured wall. Finally, it should be noted that while inertia forces have been neglected, these and other dynamic effects need to be considered in further treatments of the problem.

12. Acknowledgements

This work was sponsored by the Pipeline Research Committee of the American Gas Association (Project NG 18).

13. Appendix

Summary of Numerical Expressions and List of Symbols

TABLE 1A

Summary of numerical expressions for modeling crack extension and propagation in a pipe

A. Crack extension	
Criterion:	
Crack extension corresponds to critical stress intensity;	$K_c \equiv \sigma(\pi C^*)^{\frac{1}{2}}\varphi$
Plasticity correction: Equation (14)	$\varphi = \left(\frac{\pi\sigma}{2\bar{\sigma}}\right)^2 \ln\left(\sec\frac{\pi\sigma}{2\bar{\sigma}}\right)^2$
Plastic deformation; Equation (12)	$\bar{\sigma} = \bar{\sigma}_s$
Contribution of bulging to stress intensification; Equations (7), (10), (1), (6) and (8)	$\sigma = M\sigma_H,\ \sigma_H = \frac{P_e R}{t},\ P_e = P_c = P_L$ $M = \left[1+1.61\frac{C^2}{Rt}\right]^{\frac{1}{2}}$
Critical flaw size; (Equations (1A)–(7A))	$C^* = \frac{K_c^2 t^2}{P_L^2 M^2 R^2 \pi\varphi}$

(continued on p. 12)

★ Note that the calculations, Figure 7a, are for pipes pressurized to a fixed fraction of the yield strength (hoop stress equal to 72% of yield strength) while the data (Figure 7b) involve progressively lower fractions of yield for the higher strength levels. Presumably, the measurements would have shown a greater yield strength dependence of crack speed if the fraction of yield were a constant.

B. Crack propagation

Criterion:

Shear crack propagation proceeds with constant COD; Equations (13) and (14)	$\frac{K_c^2}{\bar{\sigma}} = \frac{\sigma^2 \pi C \varphi}{\bar{\sigma}}$
Plasticity correction	$\varphi = \left(\frac{\pi\sigma}{2\bar{\sigma}}\right)^2 \ln\left(\sec\frac{\pi\sigma}{2\bar{\sigma}}\right)^2$
Rate-sensitive plastic deformation; Equations (11) and (12)	$\bar{\sigma} = \bar{\sigma}_s + F\left(\frac{\Delta\varepsilon}{\Delta x}\right) U$
Contribution of bulging to stress intensification; Equations (7), (1), and (9)	$\sigma = M\sigma_H, \ \sigma_H = \frac{P_e R}{t}$
	$M = \left[1 + 1.61\frac{C^2}{R^2}\left(50\tanh\frac{R}{50t}\right)\right]^{\frac{1}{2}}$
Axial and radial decompression; Equations (1C) and (6)	$P_e = P_L\left[1 - 0.72\frac{(C-C^*)}{(C_{ss}-C^*)}\left(1 - \frac{U}{1500}\right)\right]\left[1 - \frac{BU}{1100}\right]^2$
Bulging; Equation (2)	$B = \beta_1\left(\frac{P_e R}{Et}\right)^m\left(\frac{c}{t}\right)^n$
Steady state; Equation (4)	$U_{ss} \equiv U_{(C=C_{ss})}$
	$C_{ss} = \beta_2\left(\frac{R}{B}\right)$

TABLE 2A

List of symbols

B	bulge deflection, $B \equiv \delta/C$
β_1	numerical coefficient describing bulging; Equation (2)
β_2	numerical coefficient describing steady-state crack length; Equation (4)
β_3	numerical constant distinguishing between plane strain and plane stress; Equation (13)
C	crack half-length
C^*	critical crack (half) length for crack extension
C_{ss}	steady-state crack length
COD	crack opening displacement
COD*	critical crack opening displacement for crack extension
δ	peak bulge or beam deflection
E	Young's modulus
$\dot{\varepsilon}$	plastic strain rate
$(\Delta\varepsilon/\Delta x)$	effective crack tip plastic strain gradient
F	linear rate coefficient
K_c	fracture toughness (critical stress field intensity for crack extension)
M	Coefficient describing contribution of bulging to local stress intensification
m	exponent in bulging equation, Equation (2)
n	exponent in bulging equation, Equation (2)
P	gas pressure
P_c	gas pressure in the vicinity of crack tip
P_e	effective gas pressure acting on bulging pipe wall
P_L	line pressure prior to failure
R	pipe radius
σ	normal stress
σ_H	hoop stress
σ_Y	yield stress
$\bar{\sigma}$	flow stress
$\bar{\sigma}_s$	static flow stress
t	pipe wall thickness
U	crack speed
U_g	speed of a decompression wave in the gas
U_R	radial velocity of the pipe wall
U_{ss}	steady-state crack speed
U_w	speed of the wall of a pressurized container
φ	plasticity correction

REFERENCES

[1] A. R. Duffy, Full-Scale Studies, *Symposium on Line Pipe Research*, American Gas Association Report, Catalogue No. L30000, March (1966).
[2] G. M. McClure, A. R. Duffy and R. J. Eiber, Fracture Resistance of Line Pipe, *J. Eng. Ind.*, 87B (1965) 265.
[3] G. M. McClure, R. J. Eiber and A. R. Duffy, *Investigation of Full-Scale Fracture Characteristics of Line Pipe and Correlation With Laboratory Tests*, Phase Report to American Gas Association, March 31 (1963).
[4] A. R. Duffy, G. M. McClure, R. J. Eiber and W. A. Maxey, *Fracture Design Practices for Pressure Piping*, Academic Press; H. Liebowitz, *Fracture*, 5 (1969) 160.
[5] A. R. Duffy, R. J. Eiber and W. A. Maxey, *Recent Work on Flaw Behavior in Pressure Vessels*, Symposium on Practical Fracture Mechanics for Structured Steel, Warrington, England (1969).
[6] A. R. Duffy (private communication).
[7] S. P. Timoshenko and S. Woinowsky–Krieger, *Theory of Plates and Shells*, McGraw-Hill, New York (1959) p. 211.
[8] G. T. Hahn, M. Sarrate and A. R. Rosenfield, Criteria for Crack Extension in Cylindrical Pressure Vessels, *Int. J. Fracture Mech.*, 5 (1969) 187.
[9] E. S. Folias, *The Effect of Initial Curvature on Cracked Flat Sheets*, Final Report to National Science Foundation, August (1968).
[10] A. Cowan and N. Kirby, *The Application of C.O.D. Measurements to Large Scale Test Behavior*, Proceedings of the Symposium on Practical Fracture Mechanics for Structured Steel, Warrington, England (1969).
[11] R. W. Nichols, *The Use of Critical Crack Opening Displacement Techniques for the Selection of Fracture Resistant Materials*, Symposium on Practical Fracture Mechanics for Structured Steel (1969).
[12] A. R. Rosenfield and G. T. Hahn, Numerical Descriptions of the Ambient Low-Temperature, and High-Strain Rate Flow and Fracture Behavior of Plain Carbon Steel, *Trans. ASM*, 59 (1966) 963.
[13] W. G. Ferguson and J. D. Campbell, The Temperature and Strain-rate Dependence of the Shear Strength of Mild Steel, *Phil. Mag.*, 21, 169 (1970) 63.
[14] N. Fitzpatrick, Ph.D. Thesis, Imperial College (1968).
[15] J. Eftis and J. M. Krafft, A Comparison of the Initiation with the Rapid Propagation of a Crack in a Mild Steel Plate, *J. Basic Eng.*, 87 (1965) 257.
[16] C. R. Hoggatt and R. F. Recht, Phase Report on Contract G7 5-633164, Denver Research Institute (1968).
[17] P. L. B. Oxley and M. G. Stevenson, Measuring Stress/Strain Properties at Very High Strain Rates Using a Machining Test, *J. Inst. Met.*, 95 (1967) 308.
[18] A. R. Dowling and J. Harding, *Proc. Conf. of High Energy Forming*, University of Denver, Colorado (1967) 731.
[19] R. W. Rhode, Dynamic Yield Behavior of Shock-Loaded Iron from 76 to 573°K, *Acta Met.*, 17 (1969) 353.
[20] W. C. Leslie, R. J. Sober, S. G. Babcock and S. J. Green, Plastic Flow in Binary Substitutional Alloys of BCC Iron—Effects of Strain Rate, Temperature and Alloy Content, *Trans. ASM*, 62 (1969) 690.
[21] M. F. Kanninen, A. K. Mukherjee, A. R. Rosenfield and G. T. Hahn, *Mechanical Behavior of Materials Under Dynamic Loads*, Springer-Verlag, ed. U. S. Lindholm, The Speed of Ductile-Crack Propagation and the Dynamics of Flow In Metals, New York (1968) 96.
[22] G. T. Hahn, M. F. Kanninen and A. R. Rosenfield, Chapman and Hall, Ltd., London, eds. P. L. Pratt *et al.*, Ductile Crack Extension and Propagation in Steel Foil, *Fracture* (1969) 58.
[23] A. R. Duffy, R. J. Eiber and G. M. McClure, unpublished full-scale test data.
[24] W. M. Catanach and F. Erdogan, Chapman and Hall, Ltd., London, eds. P. L. Pratt *et al.*, Fatigue Crack Propagation in Cylindrical Shells, *Fracture* (1969) 765.
[25] W. M. Catanach and F. Erdogan, Fatigue Crack Propagation in Cylindrical Shells, NASA Contractor Report, (1968).
[26] L. J. Copley and J. Lyell Sanders, Jr., A Longitudinal Crack in a Cylindrical Shell under Internal Pressure, *Int. J. Fracture Mech.*, 5, 2 (1969) 117.

RÉSUMÉ

On propose une analyse de la propagation instable d'une fissure de cisaillement suivant l'axe de la paroi d'un tube de grande longueur sous pression de gaz. On traite par voie numérique six processus que l'on sait associés à la propagation des fissures à savoir (1) décompression axiale du gaz, (2) gonflement de la paroi du tube, (3) décompression radiale du gaz, (4) concentrations locales des contraintes et des déformations à l'extrémité de la fissure, (5) déformation plastique, et (6) rupture ductile.

On néglige les effets dynamiques dans la paroi du tube, et l'on traite le problème en conditions quasi statiques. Comme le modèle de base comporte certaines approximations et certaines lacunes dans les descriptions numériques, on en examine plusieurs variantes. La fiabilité du modèle est testée pour diverses pressions dans le tube, diverses géométries, ainsi que pour des propriétés des matériaux différentes, et l'on compare les résultats avec les données d'essais en vraie grandeur où les fissures présentent un caractère de cisaillement total.

Il est possible d'établir une large gamme de vitesses—qui englobe les vitesses observées en pratique—correspondant aux limites dans lesquelles les paramètres du système peuvent évoluer. Les caractéristiques de gonflement et de décompression, suivant le modèle, conduisent à rendre la vitesse de propagation relativement indépendante de la

pression intérieure dans le tube. Toutefois, on observe une influence de la limite élastique et de la ténacité du matériau. Le modèle ne convient pas pour des parcours de fissuration qui s'écartent de l'axe du tube, et ne décrit pas de manière satisfaisante les conditions d'arrêt de la propagation.

Le présent mémoire constitue une première étape dans l'analyse d'un problème particulièrement complexe.

ZUSAMMENFASSUNG

Man versucht die Analyse eines unbeständigen Scherrisses, der sich axial in der Wand eines unter Gasdruck stehendes langes Rohrs ausbreitet. Sehr verschiedene Methoden zur Erfassung der Rißausbreitung werden numerisch behandelt:

(1) Axiale Entdehnung des Gases
(2) Schwellen der Wand des Rohres
(3) Radiale Entdehnung des Gases
(4) Ortliche Ansteigung der Spannung und Verformung an der Spitze des Risses
(5) Plastische Verformung und
(6) Dehnbare Rißausbreitung.

Dynamische Erscheinungen in der Wand des Rohres werden nicht berücksichtigt und der Fall wird quasistatisch behandelt. Da die numerische Auswertung des Modelles verschiedene Annäherungen und verschiedene Mängel enthält, werden mehrere Varianten des Grundmodelles untersucht. Die Glaubwürdigkeit des Modells wird für verschiedene Werte des Druckes, verschiedene Dimensionen des Rohres und für verschiedene Eigenschaften des Materials geprüft und mit Versuchen in natürlicher Größe im Gebiet des reinen Scherrisses verglichen. Ein großer Anteil von Geschwindigkeiten kann im Gebiet der aufgestellten Parametern errechnet werden einschließlich die Geschwindigkeiten die in der Praxis beobachtet werden. Die Schwellungs- und Entdehnungseigenschaften des Modells verursachen eine, weitgehend vom linearen Druck unabhängige Rißgeschwindigkeit.

Jedoch hängt die errechnete Rißgeschwindigkeit von der Elastizitätsgrenze und der Zähigkeit des Materials ab.

Das Modell ermöglicht weder die Erfahrung von nicht-axialen Rissen noch die exakte Beschreibung der Möglichkeit eines Aufhörens der Rißausbreitung.

Dieser Bericht ist die erste Stufe zur Erfassung eines besonders komplexen Problems.